Journal of Geophysical Research: Earth Surface

RESEARCH ARTICLE
10.1029/2018JF004817

Key Points:
- Grain resisting forces, and not just driving forces, are controlled by protrusion
- Theories for grain resistance need to move beyond pivot angles and also use protrusion and intergranular friction
- Temporal and spatial variations in critical Shields stresses may be explained by protrusion rather than other factors

Supporting Information:
- Supporting Information S1
- Figure S1
- Figure S2
- Figure S3
- Video S1

Correspondence to:
E. M. Yager,
eyager@uidaho.edu

Citation:
Yager, E. M., Schmeeckle, M. W., & Badoux, A. (2018). Resistance is not futile: Grain resistance controls on observed critical Shields stress variations. *Journal of Geophysical Research: Earth Surface, 123*, 3308–3322. https://doi.org/10.1029/2018JF004817

Received 17 JUL 2018
Accepted 25 NOV 2018
Accepted article online 3 DEC 2018
Published online 15 DEC 2018

Resistance Is Not Futile: Grain Resistance Controls on Observed Critical Shields Stress Variations

Elowyn M. Yager[1], Mark W. Schmeeckle[2], and Alexandre Badoux[3]

[1]Center for Ecohydraulics Research, Department of Civil and Environmental Engineering, University of Idaho, Boise, ID, USA, [2]School of Geographical Sciences and Urban Planning, Arizona State University, Tempe, AZ, USA, [3]Swiss Federal Institute for Forest, Snow and Landscape Research WSL, Birmensdorf, Switzerland

Abstract Estimates of the onset of sediment motion are integral for flood protection and river management but are often highly inaccurate. The critical shear stress (τ_c^*) for grain entrainment is often assumed constant, but measured values can vary by almost an order of magnitude between rivers. Such variations are typically explained by differences in measurement methodology, grain size distributions, or flow hydraulics, whereas grain resistance to motion is largely assumed to be constant. We demonstrate that grain resistance varies strongly with the bed structure, which is encapsulated by the particle height above surrounding sediment (protrusion, p) and intergranular friction (ϕ_f). We incorporate these parameters into a novel theory that correctly predicts resisting forces estimated in the laboratory, field, and a numerical model. Our theory challenges existing models, which significantly overestimate bed mobility. In our theory, small changes in p and ϕ_f can induce large changes in τ_c^* without needing to invoke variations in measurement methods or grain size. A data compilation also reveals that scatter in empirical values of τ_c^* can be partly explained by differences in p between rivers. Therefore, spatial and temporal variations in bed structure can partly explain the deviation of τ_c^* from an assumed constant value. Given that bed structure is known to vary with applied shear stresses and upstream sediment supply, we conclude that a constant τ_c^* is unlikely. Values of τ_c^* are not interchangeable between streams, or even through time in a given stream, because they are encoded with the channel history.

1. Introduction

Sediment transport in rivers impacts the stability of hydraulic structures and rates of sedimentation, which in turn partly control flooding hazards and river migration. Calculating the coupling between orogen erosion and solid-Earth dynamics also requires accurate sediment flux predictions. Despite over 100 years of research on bedload transport, sediment flux estimates are often incorrect by many orders of magnitude partly because of large uncertainties in τ_c^* (dimensionless shear stress that initiates sediment motion; e.g., Buffington & Montgomery, 1997). Variations in empirical values of τ_c^* between different streams are usually ascribed to differences in (a) definitions of the onset of motion, (b) methods to quantify τ_c^*, (c) bed grain size distributions, or (d) flow hydraulics in steep streams that alter the forces applied to particles (e.g., Buffington & Montgomery, 1997; Kirchner et al., 1990; Lamb et al., 2008; Recking, 2009).

Instead of using empirical τ_c^* values, many studies have estimated τ_c^* through a balance of driving forces and resisting forces (F_R). Driving force impacts on τ_c^* have received considerable attention through parameters such as protrusion (p; e.g., Isbash, 1936; Kirchner et al., 1990; Masteller & Finnegan, 2017; Schmeeckle et al., 2007) or turbulence fluctuations. The magnitude and duration of drag and lift force fluctuations can control whether sediment entrainment occurs (e.g., Diplas et al., 2008; Schmeeckle, 2015). Such effects of turbulence have often been incorporated into force balance, impulse, and energy equations for the onset of sediment motion (e.g., Lamb et al., 2008; Valyrakis et al., 2013). For almost a century, F_R has been simply modeled as a function of a grain's weight and the angle through which it pivots to leave its resting pocket (Fenton & Abbott, 1977; Li & Komar, 1986; Wiberg & Smith, 1987). Such F_R and resulting τ_c^* calculations do not include the effects of bed structure such as grain interlocking, porosity, or burial, which are hypothesized to be important in sediment transport (e.g., Allan & Frostick, 1999; Hodge et al., 2013; Sanguinito & Johnson, 2012) and granular friction (e.g., Chaudhuri et al., 2010; Song et al., 2008) literature. Without a theory for F_R that incorporates these effects, τ_c^* from force, impulse, or energy balance predictions may be inaccurate, and the sources of τ_c^* variability remain uncertain. If τ_c^* is controlled by unquantified factors such as bed structure, each τ_c^* could

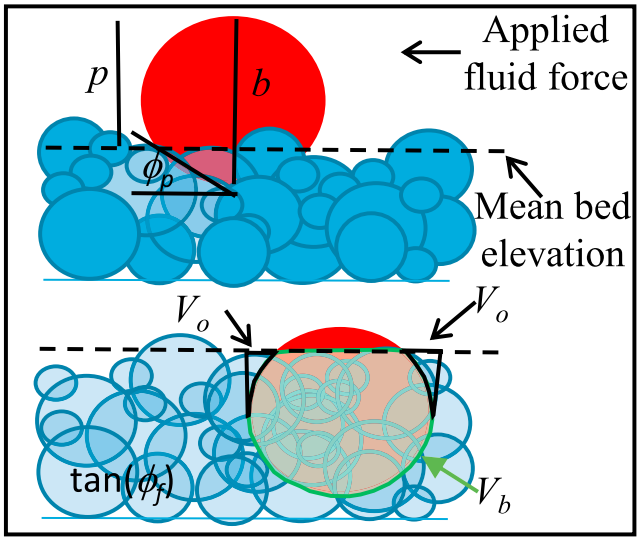

Figure 1. Variables in our theory shown in cross sections of a three-dimensional bed. The bottom diagram has a lower p to illustrate volumes.

be uniquely representative of certain channel conditions and therefore not broadly applicable between streams as commonly assumed.

Recent studies have also shown a perplexing change in empirical values of τ_c^* over time in a given river or laboratory experiment (e.g., Haynes & Pender, 2007; Hodge et al., 2013; Johnson, 2016; Masteller & Finnegan, 2017; Ockelford & Haynes, 2013; Paphitis & Collins, 2005; Reid et al., 1985; Turowski et al., 2011). Such τ_c^* variations are usually hypothesized to be driven by temporal fluctuations in the parameters that control driving forces (e.g., protrusion and bed roughness). Changes in bed structure and F_R have also been invoked to explain temporal disparities in τ_c^* (e.g., Hodge et al., 2013; Masteller & Finnegan, 2017; Ockelford & Haynes, 2013). However, few measurements of the parameters that control F_R have been made, and the importance of grain resistance variations on τ_c^* have not been explicitly quantified.

We therefore focus on answering the following fundamental research questions: (1) What controls grain resistance to motion, (2) can a theory that incorporates the effects of bed structure improve predictions of grain resistance over current formulations, and (3) can the wide spatial and temporal variations in empirical values of τ_c^* be attributed to changes in bed structure and thus F_R? To answer these questions, we (1) develop and test a novel theory for F_R that can be applied to any gravel-bedded river, (2) measure F_R in laboratory experiments and in three field sites for grains that are packed and partly buried, (3) estimate F_R for spheres that are partly buried by other spheres using a Discrete Element Method (DEM) model, (4) use these laboratory, field, and numerical modeling data to elucidate the primary controls on F_R, and (5) use our theory and a field data compilation to elucidate the controls on variations in empirical τ_c^* values. Here we use a force balance approach without taking into account the effects of turbulence for the simplicity of understanding grain resistance effects. The combined effects of grain resistance and turbulence will be important for any other calculations of sediment entrainment such as those based on grain impacts, flow impulse, and flow energy.

2. Theory for F_R

We assumed that F_R for an individual grain is controlled by the following three forces: (1) grain weight, (2) weight of sediment overlying the particle of interest, and (3) an intergranular friction force with surrounding sediment. In all of our force calculations, we assumed that the local bed is horizontal and all grains are spherical. Spheres are used in most sediment force balances (e.g., Buffington et al., 1992; Hodge et al., 2013; Kirchner et al., 1990; Lamb et al., 2008; Wiberg & Smith, 1987), which enables the use of simple geometric equations, and we return to this assumption later. We assume pivoting motion, but if pure sliding occurs, which can be common for larger grains moving over finer sediment, modifications to our equations are needed. A distribution of values for a given parameter is denoted by i, j, or k.

2.1. Force Due to Grain Weight (Formulation Used in Previous Estimates of Grain Resistance)

The force (F_g) necessary to pivot the weight of the ith grain (ranges from 1 to N = number of sampled grains) on the bed in the streamwise direction is

$$F_g(i,j) = \frac{g\rho_s(i)\pi b(i)^3}{6}\tan\left[\phi_p(i,j)\right], \tag{1}$$

for each jth percentile (from 1 to 100 in steps of 1) of the potential pivot angle (ϕ_p) distribution (Figure 1). Equation (1) includes the sediment density (ρ_s), gravitational acceleration (g), and volume of grain i, which is a function of the intermediate grain axis (b). All of our measurements are for unsubmerged grains, but if particles are under water, our force equations need to be modified to account for submerged sediment weights. The exact ϕ_p of each grain is unknown and is estimated as a distribution of potential values using

$$\phi_p(i,j) = [30 + 0.5j][b(i)/b_{50}]^{0.3}, \tag{2}$$

which was derived by Kirchner et al. (1990) and where b_{50} is the bed median grain size.

Equation (2) was determined by randomly placing natural grains on glued sediment beds and then tilting the bed until the grains rolled out of their resting pockets; it does not include the effects of grain burial and intergranular friction. Equation (2) is technically only valid between the 10th and 70th percentiles of the ϕ_p distribution, but given the paucity of equations available to predict ϕ_p for natural beds, we assume that it applies to the entire ϕ_p distribution. We revisit this assumption in section 4. Equation (1) with ϕ_p defined from equation (2) is how grain resistance is almost always currently represented in initial motion calculations, and we test this equation below.

2.2. Force Due to Partial Burial

Following the form of equation (1), the force necessary to overcome the resistance from partial burial by the sediment weight (F_s) on top of the ith grain is

$$F_s(i,j) = g\rho_s(i)[1-\lambda]V_0(i)\tan\left[\phi_p(i,j)\right], \tag{3}$$

for the jth ϕ_p, and in which λ is bed porosity and V_o is the overlying sediment volume (Figure 1), which is determined by spherical grain geometry (see Yager et al., 2007, for derivation of similar volume formulas through integration equations for spheres),

$$V_0(i) = \left(\frac{b(i)}{2} - p(i)\right)\left[b(i)^2 - \pi\left(\frac{b(i)^2}{2} + \frac{b(i)p(i)}{3} - \frac{p(i)^2}{3}\right)\right]. \tag{4}$$

No sediment burial weight is calculated if less than half of b is buried. We assume that the overlying sediment is subject to the same pivoting resistance as the grain of interest. Equation (3) represents a minimum value because it does not account for force chain extension from the overlying sediment to surrounding grains.

2.3. Force Due to Intergranular Friction

The friction and displacement force of surrounding sediment (F_d) for the kth (ranges from 1 to K, 200 here) possible internal friction angle (ϕ_f) for each ith grain is

$$F_d(i,k) = g\rho_s(i)V_b(i)\tan[\phi_f(i,k)][1-\lambda]C_V, \tag{5}$$

where ϕ_f in the granular friction literature typically represents the combined effects of grain arrangement (e.g., imbrication and clustering) and shape and bed porosity, cohesion, and/or grain size distribution on intergranular friction. It is different from ϕ_p, which here is only the angle through which a grain pivots and includes none of these intergranular resistance effects (Figure 1). Equation (5) includes both frictional sliding resistance past other grains and the displacement and plowing of downstream sediment by the ith grain when it moves. We do not imply that downstream sediment plowing occurs frequently in nature; rather, equation (5) simply states this downstream sediment weight initially resists the movement of the ith grain. Displacement of downstream sediment occurred when manually pushing on grains with a load cell and in our numerical model (see below) and must be included in our theory. The buried volume (V_b) of the ith grain is

$$V_b(i) = \pi(b(i)-p(i))^2\left(\frac{b(i)}{2} - \frac{b(i)-p(i)}{3}\right). \tag{6}$$

In equation (5), C_V is a volume correction ratio to account for more downstream sediment resisting the movement of the ith grain than just V_b. We first assumed that as a grain moves out of its pocket (one grain diameter), it displaces a downstream volume of sediment equivalent to V_b. However, in our DEM model simulations (see below), we observed that a grain actually displaces more sediment than just its buried volume, because of a cascading effect of the downstream sediment further displacing other grains (see Supporting Information S1 and Video S1). We used these DEM simulations to empirically determine a constant value of C_V (see section 3.4); it is not used as a calibration parameter. The distribution of F_R for each grain is given by the sum of F_g, F_s, and F_d. Then the distributions of F_R for all i grains are combined to create one F_R distribution for the entire bed.

Table 1
Stream Characteristics

Stream	Reynolds Creek	Sihl River	Erlenbach
Slope (%)	3	0.9	10
# rocks sampled	99	130	139
b_{50} (mm)	25	25	21
Median p (%)	50	65	34

3. Methods for Measuring, Modeling, and Predicting Grain Resistance

We used field and laboratory measurements and a DEM model to estimate F_R and test our theory for a wide range of possible channel bed conditions. The DEM simulations determined F_R for the simple case of a sphere buried by other spheres and also were used to estimate C_V in our theory. The laboratory measurements added complexity by having a sphere buried by either sand or gravel, and the field measurements used in situ natural sediment.

3.1. Field Measurements

We conducted measurements in Reynolds Creek, Idaho, United States, and the Sihl River and Erlenbach in Switzerland (Table 1). In each of these streams, we pushed on unsubmerged grains at the center of their upstream exposed areas with a load cell (oriented parallel to the bed; FUTEK LSB210, accuracy 0.001%, 100 Hz) until the grains moved out of their pocket in the streamwise direction. The maximum measured force was used as F_R and is an accurate estimate of sediment resistance to motion (e.g., Buxton et al., 2015; Hodge et al., 2013; Johnston et al., 1998; Prancevic & Lamb, 2015). Grains were on a regularly spaced grid in areas with very low local slopes, and only those with partly or fully exposed upstream surfaces and masses less than the load cell maximum (2.1 kg; weight of about a 115-mm-diameter grain) could be measured.

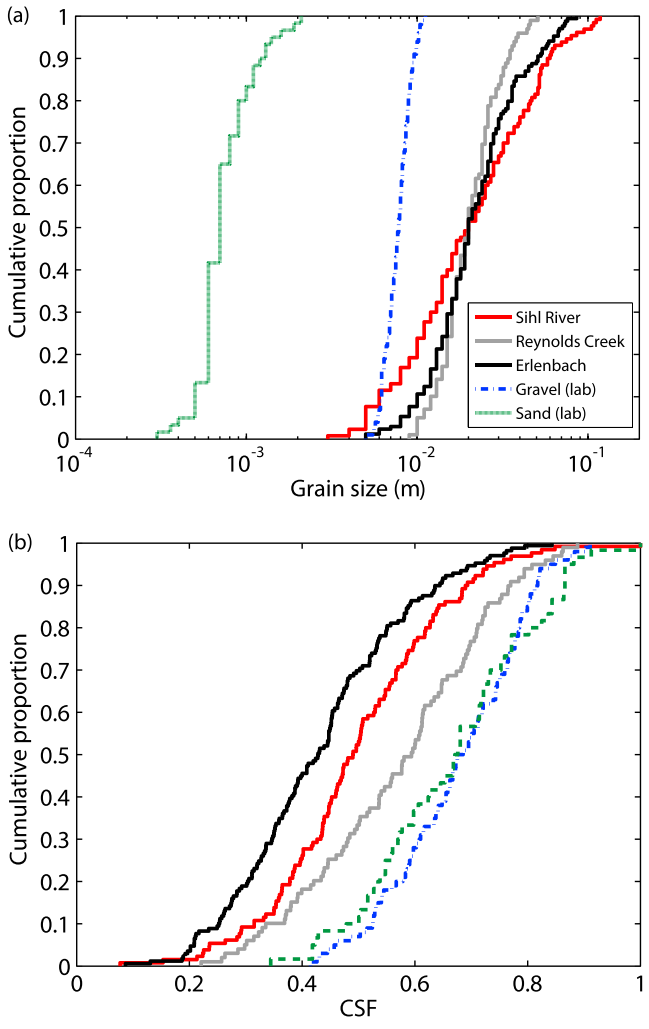

Figure 2. Measured cumulative distributions of (a) grain size and (b) CSF for the grains subjected to force measurements in the Erlenbach, Sihl River, and Reynolds Creek. Figures also show grain size and CSF distributions for the gravel and sand used to bury the test sphere in the laboratory. CSF = Corey Shape Factor.

We measured the grain mass (to 0.1 g), primary axes, and p, which was determined using a ruler from the visually estimated mean bed elevation immediately downstream of a grain to the grain top (the highest point). The downstream p was usually smaller than (or equal to) the upstream p and therefore was what likely impeded grain motion. The downstream p was often smaller because of grain imbrication and/or preferential sediment deposition downstream of certain grains. We calculated the Corey Shape Factor (CSF; e.g., Dietrich, 1982) using the measured axes of each grain. Figure 2 shows the size and CSF distributions of particles for which we measured F_R. Note that these grain size distributions may not represent those of the entire bed surface, which will be considerably wider and include both coarser and finer (e.g., sand and smaller) sizes that we could not measure within the limits of the load cell.

3.2. Laboratory Measurements

We used a test sphere (b = 90 mm) that sat on a horizontal bed in the pocket created by three closely packed spheres of the same diameter (Figure S1a). We pushed on the test sphere with the load cell until it pivoted over the saddle between two bottom spheres. We created different test sphere p by burying it to various degrees with sand or gravel and measured forces for each p 5–6 times to establish means.

3.3. Numerical Model

We used LIGGGHTS within the LAMMPS DEM model software (Kloss et al., 2012) with periodic boundary conditions and the same formulations for frictional forces and parameter values as in Schmeeckle (2014). The simplified Hertz-Mindlin contact model controls the forces and torques between overlapping spheres; see Schmeeckle (2014) for more details and specific equations used. All parameters were held constant between DEM model simulations except p, and we used the following values for sediment density (2,650 kg/m^3), Young's modulus

(1×10^{-7} Pa), Poisson's ratio (0.45), coefficient of restitution (0.1), coefficient of friction (0.6), and coefficient of rolling friction (0.01). All DEM model runs were conducted before comparison to our theory; none of the DEM model parameters were adjusted to better match F_R with our theory. The modeling domain was 0.0387, 0.02, and 0.075 m in the streamwise, lateral, and vertical directions, respectively. A test sphere sat on a horizontal bed of three closely packed fixed spheres of identical diameter (b = 10 mm; Figure S1b). We randomly added and settled smaller spheres (mean and standard deviation in b of 0.9 and 0.1 mm, respectively) to fully bury the test sphere. We then numerically removed the smaller spheres above given elevations to create five different test sphere p values between runs.

In each run we incrementally increased an applied constant bed-parallel, streamwise force until the sphere pivoted out of its pocket. The force was applied to the center of mass of the test sphere, and this F_R was verified for a test sphere without burying small spheres using equation (1) and ϕ_p calculated from bed geometry (19°, closely packed sphere pocket geometry). We used a relatively constant ϕ_p in all of our simulations to determine the importance of p independent of variations in ϕ_p, the effects of which on grain motion have already been extensively studied (e.g., Buffington et al., 1992; Kirchner et al., 1990; Li & Komar, 1986). However, this angle was not completely constant; as the test sphere became more buried (very low p), the angle through which it needed to pivot visually appeared to slightly increase because of the additional sediment impeding its movement. The effects of slight changes in ϕ_p are further discussed in section 4. We normalized each F_R by the respective particle weight for most of our results.

3.4. F_R Predictions

We tested the predictions of F_R from our theory (equations (1)–(6)) using the estimated values from the field, laboratory, and DEM simulations. In all of our calculations, we treat ϕ_f, ϕ_p, and p as independent parameters, which is partly supported by the lack of correlation between ϕ_p and p for individual grains (Kirchner et al., 1990). We predicted F_R for the laboratory and DEM data using the known values of b, p, and ϕ_p (19°, assumed constant with p). We varied the value of ϕ_f between predictions through the range of known values in the literature for gravel, sand, and spheres (see section 4).

For field F_R predictions, we used the measured values of b and p for each grain and the potential distribution of ϕ_p for each grain from equation (2). We varied ϕ_f between predictions using known values for alluvial sediment (see section 4), but in this case we used a distribution of potential values of ϕ_f in each prediction rather than a single value as in the DEM and laboratory calculations. In real streams, ϕ_f could spatially vary as a function of parameters such as local grain arrangement and shape. Therefore, we randomly sampled it from a normal distribution (limits of 0–89°) with a certain mean and standard deviation of ϕ_f to obtain the potential ϕ_f distribution for each grain. We changed the mean ϕ_f between predictions.

In each river, our theory results in distributions of possible F_R values for a given grain because we do not know the exact values of ϕ_f and ϕ_p and must use potential distributions for these parameters. We used all possible combinations of ϕ_f and ϕ_p values to obtain the F_R distribution for a given grain and then combined these distributions for all grains on the bed to yield the F_R distribution for a given stream. We also tested the commonly accepted formulation for grain resistance that is used in force balance calculations of the onset of motion, which is equation (1) alone. For use of this equation alone, we similarly obtained the potential distribution of ϕ_p for each grain using equation (2) and then combined the F_g distributions for all grains on the bed to yield the F_R distribution for a given stream.

The value of C_V for all of our predictions (field, laboratory, and DEM) was determined from our DEM model. It was calculated in each simulation using the known volume of spheres downstream of the test sphere that were displaced by the test sphere when it just moved out of its pocket. This volume was divided by V_b, which was calculated using equation (6), and the resulting value of C_V (4.8 ± 0.3) was the average value from all five DEM model simulations because C_V did not systematically vary with p. For the field, we assumed λ = 0.4, whereas we used the measured values of 0.36 and 0.44 in the laboratory and DEM predictions, respectively. Sensitivity analyses demonstrated that small uncertainties in λ had relatively little impact on prediction accuracy (see Supporting Information S1). We note that the only parameter we varied in our theory to match the measured/simulated F_R values was ϕ_f.

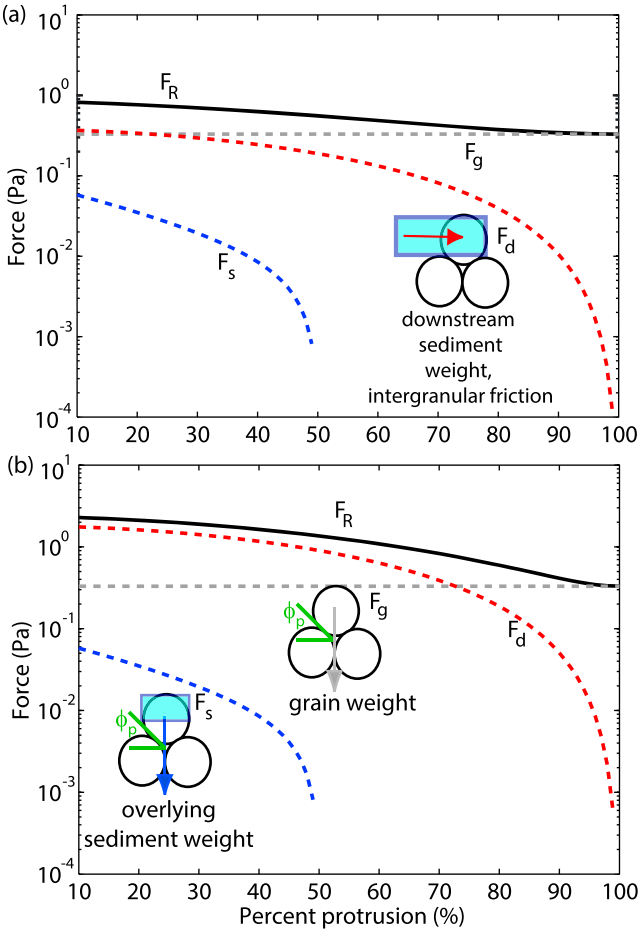

Figure 3. Median values of each component of our theory (F_g, F_s, and F_d) and the total of all components (F_R) as functions of percent p when the mean ϕ_f is (a) 30° or (b) 70°. Cartoons to the left of forces show parameters that contribute to each force component. In the cartoons, sediment is entrained from right to left. The blue boxes represent sediment burying the grain of interest and are shown as boxes for simplicity although their shapes can be more complex (see equations for volumes in text).

4. Results

4.1. Importance of Various Force Components in our Theory

We first conducted a sensitivity analysis on the influence of p and ϕ_f on each force component of our theory for a theoretical value of b_{50} (assumed $b = b_{50}$ here). We calculated the median values of F_R, F_s, F_g, and F_d for a given percent p (varied between 10% and 100%) with two end members of the possible ϕ_f distribution (mean value of 70° vs. 30°, each with a standard deviation of 15°). Most of the forces (F_R, F_s, and F_d) increased with smaller p (greater burial) (Figure 3) because p determines the portion of the grain that experiences intergranular friction and the volumes of overlying sediment and resisting downstream sediment. As shown in equation (1), F_g is independent of p. Regardless of the value of p and ϕ_f, F_s was the smallest force, often by at least an order of magnitude, and was zero when percent $p \leq 50\%$. The relative magnitudes of F_g and F_d depended on p and ϕ_f, with F_g becoming more important as p increased (grain is more exposed) or ϕ_f declined (less intergranular friction; Figure 3).

4.2. Empirical Observations of Parameters that Control F_R

A direct relation between p and F_R occurred in field, laboratory, and DEM data (Figure 4a). For a given p, F_R generally increased as grain shape became flatter (lower CSF) from spheres to gravel. The highest F_R occurred for real riverbeds, which were composed of natural grains with low CSF and a wide range of grain sizes (Figure 4a). Such changes in F_R with particle shape and grain size are supported by the granular friction literature (e.g., Farhadi & Behringer, 2014; Trulsson, 2018) and imply that ϕ_f is an important control on grain resistance to motion.

4.3. Predictions of F_R for Field, Laboratory, and DEM Data

Resisting forces were predicted well by our theory for a sphere partly buried by other spheres, sand, and gravel when ϕ_f was about 10–15°, 30–35°, and 45–50° (Figure 4b), respectively, which mostly correspond to ϕ_f values in the literature for each sediment type (e.g., Culshaw et al., 1991; Mollanouri Shamsi & Mirghasemi, 2012). Our theory also generally predicted the observed increase in F_R with lower p for a given bed, which could not be calculated with equation (1) alone because it does not account for the effects of grain burial. Equation (1) predicts a constant value of F_R for all p equal to that predicted by our theory at 100% p. Small deviations from measured values may be partly from assuming spherical grains in our theory and a constant ϕ_p with different levels of grain burial; ϕ_p may be higher for very low p because of the large relative height of the downstream grains that impeded pivoting. For example, if we had allowed ϕ_p to slightly increase with p in our predictions of the DEM data, we would have better approximated the F_R values for very low p. In addition, we assumed C_V was constant, but it will likely change with λ and bed grain size in the field and laboratory because these parameters will alter the volume of grains on the bed at any location.

For the field data, when we used the currently applied resistance formulation in force balance models, equation (1) alone, F_R was systematically underestimated for all percentiles of its distribution in all three streams (Figure 5). To predict the field data with our theory, we varied the mean ϕ_f through the published range of values for river sediments (31–67°) measured using strength tests (e.g., Chang & Cheng, 2014; Lin et al., 1998). Low percentiles (0–30%) of the F_R distribution were generally predicted well by our theory in all three field sites as long as $\phi_f > 30°$, with ϕ_f as a single value or as the mean within a distribution (Figure 5). Therefore, low percentiles of the F_R distribution can be estimated even if the exact value or distribution of values for ϕ_f is uncertain. Such low percentiles are important because they determine the onset of motion of a streambed and the movement of these grains subsequently alters the resisting forces for other sediment.

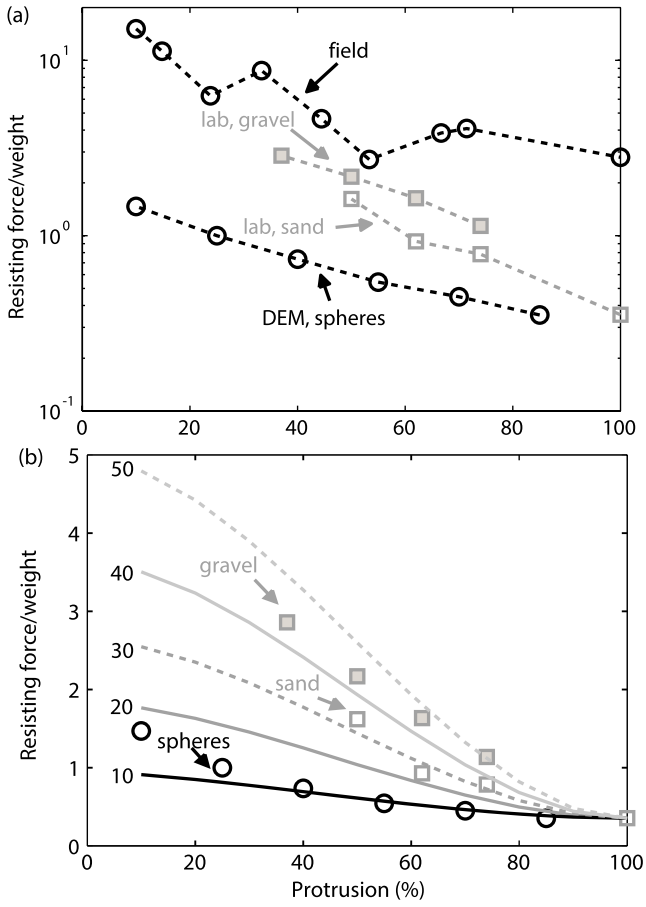

Figure 4. (a) Normalized F_R as a function of p for spheres partly buried by spheres (DEM), sand (laboratory), and gravel (laboratory). Normalized median F_R from all three field sites combined (sample size not large enough at some sites to show relation) were calculated from values binned at 10% p intervals. The median measured p within each 10% interval is shown. Two data points at 80% and 90% p bins were excluded because they only contained a single measurement and a median could not be calculated. (b) Laboratory and DEM data (symbols) with predicted normalized F_R from our theory (lines) labeled with the single value of ϕ_f used. DEM = Discrete Element Method.

We found through sensitivity analyses that most predicted F_R (up to the 70th percentile of distribution) were relatively insensitive to the standard deviation of ϕ_f. However, a range of ϕ_f values with a mean of about 66° generally allowed for accurate predictions of the entire F_R distribution in two out of three streams (Figures 5a and 5b). In the remaining stream (Erlenbach), our theory generally underestimated F_R (Figure 5c) because this channel contains highly angular, poorly rounded sediment and large amounts of silt and clay (which increases cohesion). Most ϕ_f do not include the combined effects of very angular grains and cohesion (e.g., Chang & Cheng, 2014; Lin et al., 1998) and may therefore be lower than what could occur in the Erlenbach, which could partly explain our slightly underestimated F_R. Our ϕ_f are also at the upper end of the range of those measured from strength tests because we pushed on single grains rather than shearing an entire box of sediment. Measured bulk resistance angles generally increase with the fewer number of potentially mobile grains used in a sample (Booth et al., 2014).

Some of the other small discrepancies between predicted and measured values of F_R in our three field sites could be caused by using equation (2) to predict the entire distribution of ϕ_p. Equation (2) is technically only valid between the 10th and 70th percentiles of the ϕ_p distribution, which implies that it would have larger errors at the distribution tails. Our theory usually had the largest prediction uncertainties for very large values of F_R (Figure 5), and such errors could be caused by inaccurate estimates of the higher percentiles of the ϕ_p distribution. We also assumed spherical grains for the volume calculations (equations (4) and (6)) in our theory, but many grains at our field sites deviated from spheres. This could be an additional source of discrepancies between measured and predicted values of F_R.

5. Discussion

5.1. Controls on Grain Resistance to Motion

The large underestimation of F_R by equation (1) (with ϕ_p from equation (2)) for even low percentiles of the F_R distribution (most easily moved grains, Figure 5) implies that the commonly employed grain resistance formulation for onset of motion calculations is incorrect. Specifically, the widely used force balance for the onset of motion implicitly includes assumptions that (a) p influences driving but not resisting forces and (b) all grain resistance can be encapsulated into a pivot angle (see section 5.2). Our measurements and theory demonstrate that ϕ_p is only a component of grain resistance, and grain burial (inverse of p) and intergranular friction (ϕ_f) are also important controls. Both p and ϕ_f caused measured (laboratory and field; Figures 4a and 5), simulated (DEM; Figure 4a), and theoretical (Figure 3) values of F_R to vary by an order of magnitude.

The use of a p distribution was also key to accurate F_R predictions. To demonstrate this, we assigned all grains in the Sihl River the same value of percent p instead of using their measured percent p. We then varied this value of percent p for all grains between predictions using our theory. The distribution of F_R was completely incorrect regardless of what single p or ϕ_f was chosen (Figure 6). Further support for the role of p in controlling F_R comes from one study that demonstrated grain overlap with other particles (similar to grain burial) impacts the forces needed to vertically dislodge a grain from a riverbed (Sanguinito & Johnson, 2012).

Our results that ϕ_f controls F_R are supported by geotechnical engineering experiments in which bulk sediment failure is partly controlled by the bed grain size distribution and porosity (λ) and grain angularity, shape, and orientation (e.g., Bagherzadeh-Khalkhali & Mirghasemi, 2009; Bareither et al., 2008; Culshaw et al., 1991; Estrada et al., 2008; Lambe & Whitman, 1969; Mollanouri Shamsi & Mirghasemi, 2012; Simoni & Houlsby, 2006;

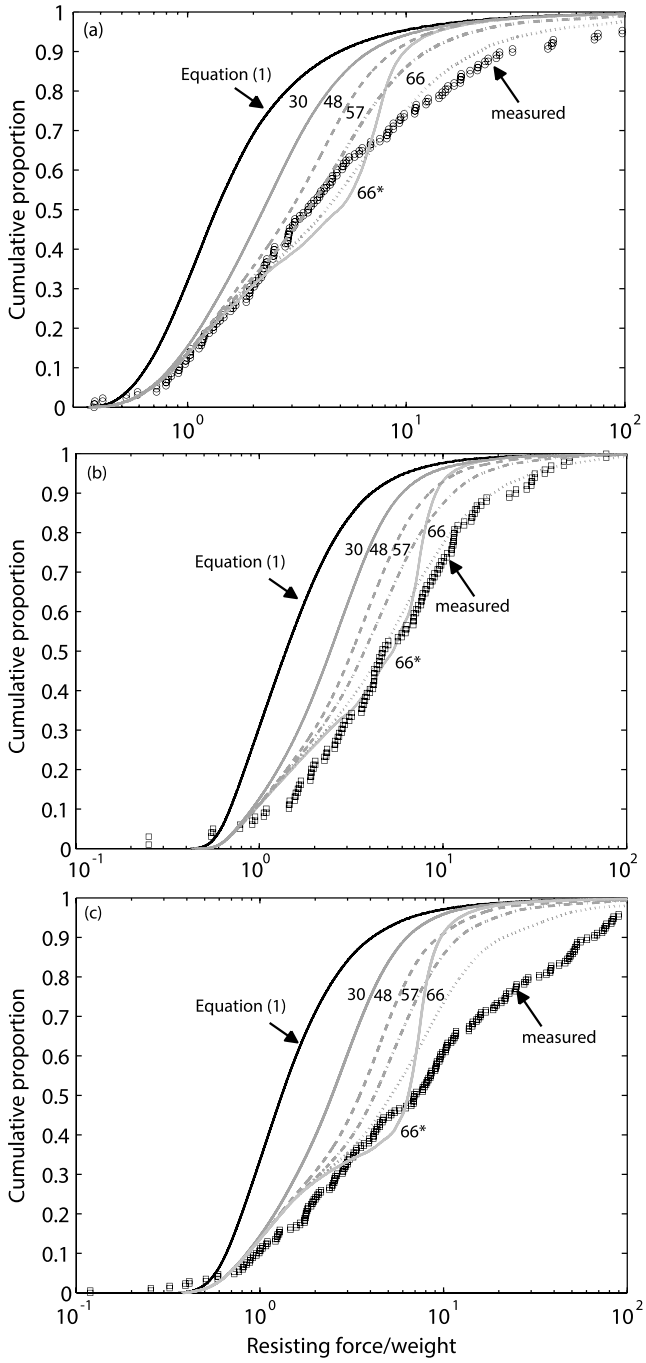

Figure 5. Measured (symbols) and predicted (lines) distributions of normalized F_R for (a) the Sihl River, (b) Reynolds Creek, and (c) Erlenbach. Predictions using our theory are labeled with the mean ϕ_f used (constant standard deviation of 15°, except for line with an asterisk, for which it was zero).

Zhuang et al., 2014). Similarly, granular physics experiments and numerical modeling results demonstrate that sediment jamming is influenced by the coordination number (average number of contacts per particle), volume fraction (1-λ), particle shape, and bed arrangement (controlled by conditioning from applied stresses, forces; e.g., Bandi et al., 2013; Bertrand et al., 2016; Bi et al., 2011; Chaudhuri et al., 2010; Ciamarra et al., 2011; Farhadi & Behringer, 2014; Kumar & Luding, 2016; Silbert, 2010; Torquato & Stillinger, 2010; Zhang et al., 2010). Finally, observations in rivers and laboratory experiments suggest that grain clustering and imbrication, as well as the abundance of fine cohesive sediment, could alter overall gravel-bed resistance to motion (e.g., Hassan & Reid, 1990; Kothyari & Jain, 2008; Perret et al., 2018; Reid et al., 1985; Strom et al., 2004).

We hypothesize that all of the parameters mentioned in the previous paragraph influence ϕ_f and explain its variation between different sediment mixtures and streams (Figures 4b and 5). Further research is needed to better quantify (a) the uniqueness and overlap between the various parameters mentioned in the geotechnical engineering, granular physics, and fluvial sediment transport literature, (b) the relation between these unique parameters and ϕ_f, and (c) the relative importance of these unique parameters in controlling F_R. We finally note that although cluster formation has been hypothesized to control sediment mobility (e.g., Hassan & Reid, 1990; Strom et al., 2004), no mechanistic theory exists to account for the influence of clusters on F_R. Our theory directly includes the parameters (ϕ_f, ϕ_p, and p) that would change F_R through cluster formation.

5.2. Uncertainties in Pivot Angle Measurements and Use

Recent studies have also suggested potential inaccuracies in ϕ_p values that are obtained by placing grains on glued beds and then tilting the beds until the grain of interest moves (e.g., Hodge et al., 2013; Johnston et al., 1998; Prancevic & Lamb, 2015). Such ϕ_p do not represent in situ grain pivoting motions that will usually involve more interactions with the surrounding bed material. Equation (2) may therefore underestimate ϕ_p for natural riverbeds. Conversely, ϕ_p values determined for in situ sediment are likely significant overestimates because they are obtained by measuring F_R using a load cell, assuming $F_R = F_g$, and then back-calculating ϕ_p using equation (1) (e.g., Hodge et al., 2013; Johnston et al., 1998; Prancevic & Lamb, 2015). Such ϕ_p values therefore indirectly incorporate the effects of burial and intergranular friction.

In theory, one could use these empirically derived in situ ϕ_p values in equation (1) to obtain F_R for different rivers. Although such a calculation would appear to be a simpler version of our theory, these ϕ_p are not broadly applicable and obscure the actual mechanics of grain resistance to motion. The in situ ϕ_p distributions strongly depend on individual grain partial burial and parameters that control intergranular friction such as porosity, angularity, and grain size distribution. For example, Hodge et al. (2013) found very different distributions of in situ ϕ_p (estimated using a load cell) depending on longitudinal locations within pools/riffles and measurement year. They hypothesized that spatial changes in ϕ_p occurred because of differences in grain exposure and packing, as well as surrounding sediment cohesion. We posit that packing and cohesion should dominantly affect, and be represented by, ϕ_f rather than ϕ_p. We have also demonstrated that protrusion, which is similar to exposure, influences F_R separate from any changes in ϕ_p. Therefore, many previously reported variations in in situ ϕ_p are likely instead driven by their back-calculation from a measured F_R that includes the impacts of different ϕ_f and p.

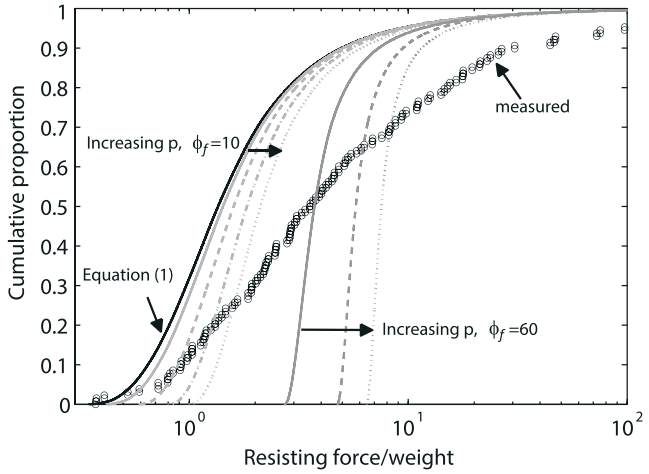

Figure 6. Demonstration of the failure of the predicted F_R distributions to match measured values when a single value of p is used, rather than the measured p distribution (as in Figure 5). Measured (symbols) and predicted (lines) distributions of normalized F_R for the Sihl River. Each line had single values of p and ϕ_f for all grains; for ϕ_f = 10° or 60°, p was varied between lines.

5.3. What Controls Spatial and Temporal Variations in τ_c^*?

The mechanistic effects of F_R on temporal and spatial variations in τ_c^* could not be previously predicted because F_R was only modeled as a function of ϕ_p, which does not have known and predictable systematic temporal fluctuations. In contrast, the reach-averaged boulder ($b > 256$ mm) protrusion can be inversely related to the relative sediment availability (Yager et al., 2007, 2012), and it is likely that p for smaller grains will also vary with fluctuations in the sediment supply. We note that a channel bed could also adjust to greater sediment supply by increasing the bed slope through simple deposition, thereby just covering all sediment on the bed, or through grain size changes (Dietrich et al., 1989; Johnson et al., 2015; Madej et al., 2009). Therefore, the exact relation between sediment supply and grain protrusion has yet to be established. Support for τ_c^* temporal variations being sediment supply dependent is also provided by the theory of Johnson (2016), who predict τ_c^* as an empirical function of transport disequilibrium measured in a set of flume experiments. Results from the granular friction literature also imply that ϕ_f (e.g., Bertrand et al., 2016; Song et al., 2008) will increase with higher fine sediment supply (alters porosity and cohesion) or with changes in grain arrangement (e.g., interlocking). Thus, p, ϕ_f, and F_R can readily vary and can mechanistically explain why τ_c^* is different between streams or through time; a constant τ_c^* is actually highly unlikely.

5.3.1. Calculation of τ_c^* Variation With Bed Structure

To demonstrate potential bed structure controls on τ_c^*, we used a force balance (Kirchner et al., 1990) to calculate the potential τ_c^* distribution for the median grain size of a synthetic channel bed ($b = b_{50} = 0.06$ m),

$$\tau_c^*(i,j,k) = \frac{F_R(i,j,k) - F_{sw}(i)\sin(\beta)}{0.5A(i)\langle f(z,i)\rangle^2\left[C_D + C_L\tan\left(\phi_p(i,j)\right)\right][\rho_s(i)-\rho]gb(i)}, \quad (7)$$

where C_D (0.4) and C_L (0.2) are drag and lift coefficients, respectively (e.g., Wiberg & Smith, 1987), κ is von Karmen's constant, ρ is water density, A is the exposed cross-sectional area of a grain (function of b and exposure), z is distance from the bed, $\langle\rangle$ denotes a vertical average, F_{sw} is the submerged grain weight, β is the channel slope, and $f(z)$ is part of the logarithmic velocity profile equation. Equation (7) follows that used by Kirchner et al. (1990), who also provide the necessary equations for $f(z)$, A, and exposure. We determined the distribution of F_R in equation (7) using the following two different methods: (i) from equation (1) with ϕ_p from equation (2) and (ii) using our complete theory (equations (1)–(6)). Values of τ_c^* using F_R from equation (1) only include the impacts of p on drag and lift forces, whereas τ_c^* values employing our theory for F_R include these driving forces and the effects of p and ϕ_f on F_R. All calculations used the submerged grain weight, which simply involved substitution of ρ_s-ρ for ρ_s in equations (1), (3), and (5).

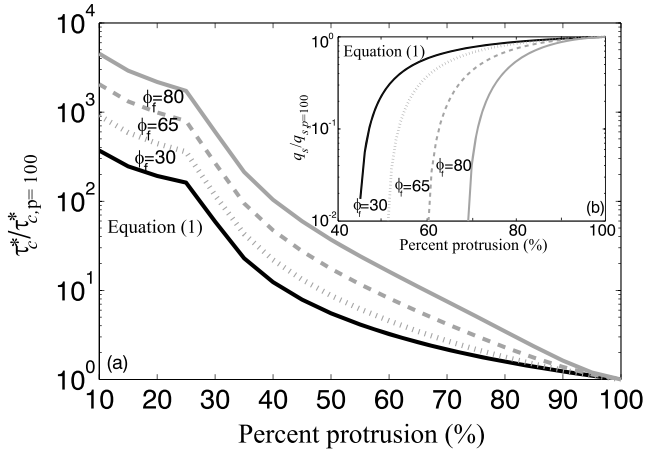

Figure 7. Theoretical variation of (a) the median τ_c^* and (b) q_s with percent p for equation (1) and our theory (labeled with ϕ_f). τ_c^* and q_s are normalized by their values when p = 100% of b.

Calculations using equation (7) yielded a distribution of potential τ_c^* values even for a single grain (one i) because distributions of ϕ_f and ϕ_p were used. To simplify the presentation of our results, we simply show the median τ_c^* for a given calculation scenario (Figure 7). Between scenarios, we systematically varied p and the mean value of ϕ_f. For each scenario, we also used these resulting median τ_c^* values in a bedload equation (Meyer-Peter & Müller, 1948) to determine the sediment flux (q_s; see Supporting Information S1). These calculated τ_c^* values are approximations of the actual entrainment threshold rather than of a higher reference shear

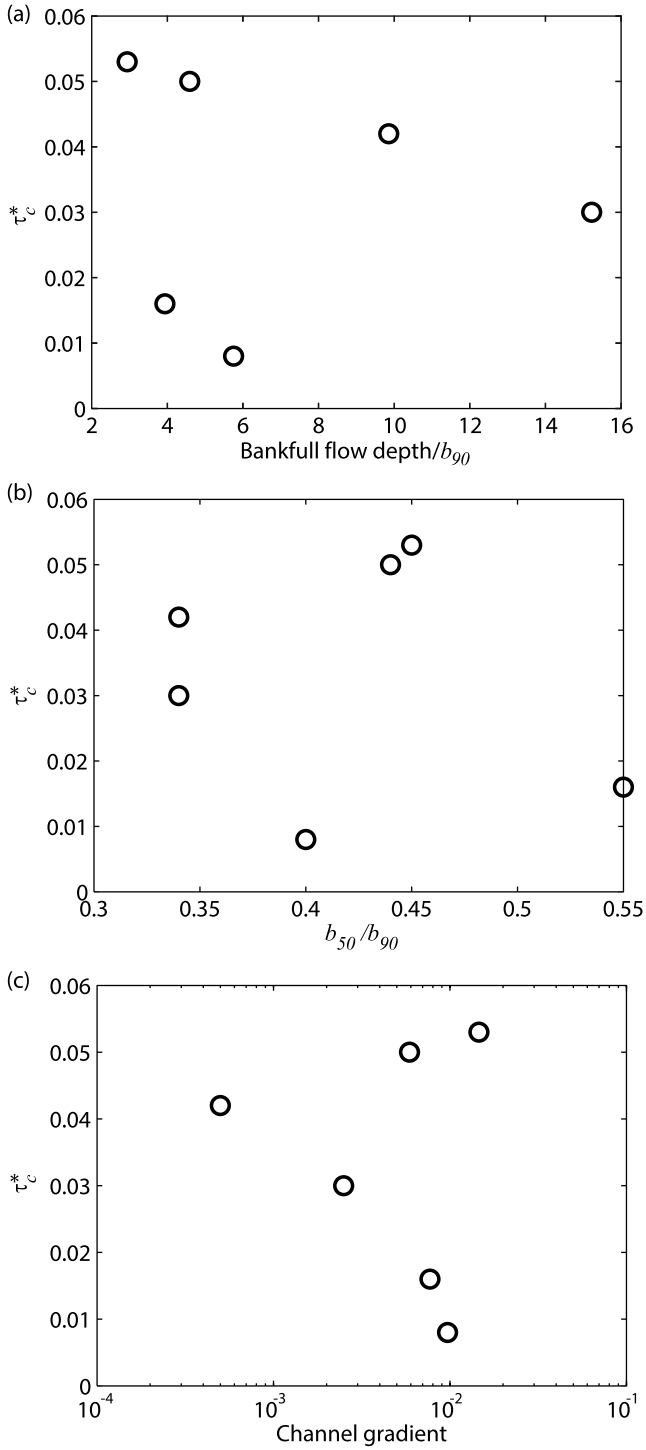

Figure 8. Compilation of empirical field τ_c^* from Mueller et al. (2005) as a function of the measured (a) relative submergence, (b) grain size distribution, and (c) slope.

stress that is part of the original bedload equation (Pähtz & Durán, 2018). In this sediment transport equation, b_{50} is the representative grain size that is used for q_s calculations for the entire bed of sediment. We calculated q_s for an applied dimensionless shear stress (τ^*) that was equal to two times the median τ_c^* from our theory when percent p = 70% and ϕ_f = 65°. We note that use of a lower τ^* demonstrated even stronger effects of p and ϕ_f on q_s and use of a different sediment transport equation will not change our overall conclusions.

If a change in bed structure decreases p, we calculated that τ_c^* will increase and q_s will decline regardless of the F_R equation used (Figure 7). Neglecting the effects of p on F_R caused τ_c^* and q_s changes with p to be systematically underestimated when compared to our theory, particularly when $\phi_f \geq 65°$ or $p \leq 60\%$. In our theory, small changes in p and ϕ_f can induce large differences in τ_c^* that are of similar magnitudes to those observed between different streams or experiments. Spatial variations in τ_c^* are often ascribed to differences in measurement methodologies, grain size distributions, or relative submergence (ratio of flow depth to particle size), but these parameters did not vary in our calculations. The observed scatter in τ_c^* may instead be induced by differences in both driving and resisting forces, which are in turn controlled by variations p and/or ϕ_f between streams or through time.

Equation (7) does not account for the influence of particle impacts, which can cause direct sediment entrainment as well as loosen a given grain (e.g., Ancey, 2010; Lee & Jerolmack, 2018; Pähtz & Durán, 2017; Vowinckel et al., 2016), thereby decreasing its resisting force and making it easier to move. Many studies have also demonstrated that drag and lift force fluctuations are actually responsible for particle entrainment (e.g., Diplas et al., 2008; Leary & Schmeeckle, 2017; Schmeeckle et al., 2007; Valyrakis et al., 2010) and that these fluctuations in lift and drag forces vary with p (Schmeeckle et al., 2007). We did not incorporate magnitudes and durations of flow turbulence into equation (7) because there is no generally applicable theory to predict how these parameters will change with p, which is necessary for accurate τ_c^* predictions. Regardless of the driving mechanism (e.g., impacts or turbulence), sediment motion cannot occur until resisting forces have been exceeded; the variations in resisting forces documented above are a fundamental control on observed τ_c^* differences. Further work is needed to incorporate simplified parameterizations of all of these processes into predictive equations for the onset of grain motion. For example, distributions of possible forces or turbulence intensities have been incorporated into force balance equations (e.g., Lamb et al., 2008; Vollmer & Kleinhans, 2007), and such modifications could also be made to equation (7) if a model for turbulence variation with p is also included. Our theory for grain resistance could also be modified for more general use in calculations of particle impact, flow impulse, flow energy, or rebound entrainment thresholds (e.g., Celik et al., 2013; Pähtz & Durán, 2018; Valyrakis et al., 2013).

5.3.2. Field Data on Bed Structure Controls on τ_c^*

Further evidence for the control of p on τ_c^* comes from a field data compilation. We used τ_c^* values from Mueller et al. (2005), who employed the same methodology to define τ_c^* in all rivers considered in their study; they extrapolated measured bedload fluxes to a reference transport rate. We limited our focus to the streams from Mueller et al. (2005) that met the following three criteria. First, they had relative submergence values (h/b_{90}; where b_{90} is the grain size for which 90% of grains are

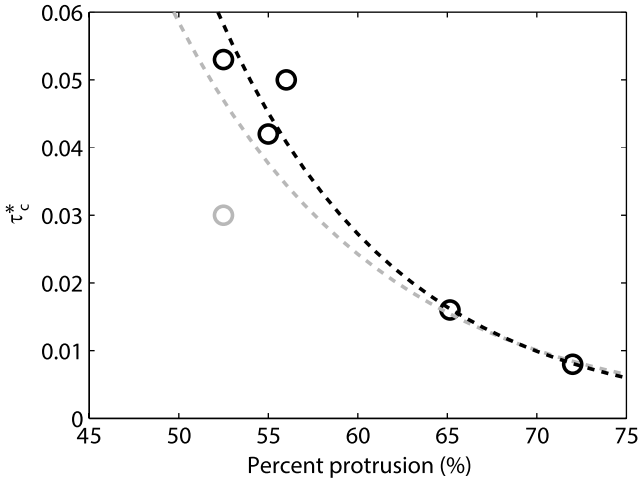

Figure 9. Variation of empirical field τ_c^* from Mueller et al. (2005) with compiled values of percent p. Lines show exponential fits to data with (gray) or without (black) the stream with large temporal variation in embeddedness (gray circle). Standard errors are not shown because most streams have two or less embeddedness measurements reported.

finer and h was for bankfull flow) ≥3 to minimize changes in velocity profiles, turbulence, and morphologic drag that are expected when relative submergence is low and which impact τ_c^* (e.g., Lamb et al., 2008). Second, each stream needed published values of cobble embeddedness (see Sennatt et al., 2006, for a review on embeddedness measurements), which is a measure of particle burial (~inverse of p). To minimize errors, we only used streams for which embeddedness was not reported to be a visual estimate (Espinosa et al., 1997; Petrosky et al., 1988; Richards & Cernera, 1987; US Bureau of Land Management, 1996; USDA Forest Service, 2002, 2005, 2014). If a stream had visual embeddedness estimates, we only used those that were calibrated to quantitative measurements. Third, we used embeddedness measured as spatially and temporally close to the bedload sampling locations and years, respectively, as possible. When embeddedness and bedload sampling did not occur at the same times, we excluded any streams if large fires occurred in the surrounding watershed between the two different measurements. Fires can alter sediment transport rates and channel bed conditions (e.g., Reneau et al., 2007), which makes concurrent sampling of embeddedness and sediment flux important. We used median values if more than one measurement of embeddedness was available at a given river and then calculated p = 1-embeddedness. The compilation resulted in six streams with both τ_c^* and p estimates (South Fork Salmon River, North Fork Clearwater Creek, Main Red River, South Fork Red River, Herd Creek, and Lolo Creek; all in Idaho, United States; see Mueller et al., 2005).

Despite having a wide range of values, these τ_c^* did not systematically vary with relative submergence, grain size distribution (b_{50}/b_{90}), or slope using the data provided by Mueller et al. (2005; Figure 8). Therefore, many of the previous explanations for scatter in τ_c^* such as differences in grain size distributions, flow hydraulics, or measurement methodology (e.g., Buffington & Montgomery, 1997; Lamb et al., 2008; Recking, 2009; Shvidchenko et al., 2001) may not always explain τ_c^* variations. In contrast, τ_c^* exponentially decreased with higher percent p (α = 0.008, R^2 = 0.87; Figure 9) and the relation between these two parameters improved (α = 0.002, R^2 = 0.98) if the one stream with large temporal variations in p (49% variation) was excluded from the fit. The remaining scatter in τ_c^* could be partly explained by using the b_{50} of each field site and reasonable mean values of ϕ_f in our theory (see Supporting Information S1). In this data set, τ_c^* varied by a factor of six with p, which is a large portion of the observed τ_c^* scatter in lower-gradient, gravel-bedded rivers. Much of the observed variation in τ_c^* could therefore caused by different p and ϕ_f between streams, which we have demonstrated using this field data compilation and our calculations in section 5.3.1.

5.4. Calculations of τ_c^* During Transport Events

Our equations represent one snapshot of the bed state before any changes have occurred to bed structure or grain size during a sediment transport event. If F_R throughout a transport event is needed, temporal changes in b, p, ϕ_p, and ϕ_f would need to be known. However, this is an issue that is not unique to our theory and is a common but rarely acknowledged problem in almost any calculation of the onset of sediment motion and sediment transport. Except for sediment transport predictions that use the Exner equation for the mass balance of individual grain sizes during an event, almost all simple calculations of the critical shear stress (e.g., assumed τ_c^* value) and bedload flux are based on the assumption that the bed grain size is constant during an event. The same problem exists with almost all previous force balance formulations for τ_c^* (e.g., Kirchner et al., 1990; Lamb et al., 2008; Wiberg & Smith, 1987), which are also implicitly based on the assumption that p, roughness (controls velocity profile), b, and ϕ_p do not change during a sediment transport event. Such assumptions are unlikely to be correct (e.g., Hodge et al., 2013; Johnson, 2016; Masteller & Finnegan, 2017). For example, if fine sediment is winnowed around larger grains at the beginning of an event, this will increase p and decrease ϕ_p, thereby causing τ_c^* of the larger grains to decrease through time. A better understanding is needed on the variation of p, ϕ_p, and ϕ_f with flow

magnitude, flow duration, and sediment supply history. If empirical relations between these bed parameters and external driving factors were developed, then the temporally varying driving forces, F_R, and τ_c^* could be predicted using our theory. Such τ_c^* values could then be employed to improve bedload transport predictions throughout flow events.

6. Conclusions

We develop and test a novel theory that provides the first quantitative predictions of the effect of particle burial and intergranular friction on individual grain resistance to motion. We use our theory to demonstrate that neglecting p and ϕ_f can cause significant underestimates of F_R and τ_c^* and overestimates of sediment fluxes. Our theory and compiled field data show that small changes in p and ϕ_f may explain part of the scatter in τ_c^* values without invoking the common explanations of differences in measurement methodology or grain size. The deviation of τ_c^* from an assumed constant value may be explained by small variations in bed structure, which in turn are likely controlled by fluctuations in sediment supply, flow history, and lithology. Landscape evolution models may need to employ a temporally and spatially variable τ_c^* to properly estimate the importance of climate and tectonics on orogen evolution. However, further work is needed to identify the key drivers of the spatial and temporal variations in the parameters that control grain resistance.

Symbol definitions

A	bed-perpendicular area of grain exposed to flow
b	grain diameter
b_{50}	median grain size of bed
b_{90}	grain size for which 90% of grains are finer
C_D	drag coefficient
C_L	lift coefficient
e	exposure
F_d	force caused by friction by, and displacement of, sediment surrounding grain of interest
F_g	force necessary to pivot weight of grain of interest
F_R	total resisting force, $= F_g + F_s + F_d$
F_s	force from sediment weight that overlies grain of interest
F_{sw}	force from submerged weight of the grain of interest
$f(z)$	part of logarithmic velocity profile equation
g	gravitational acceleration
h	bankfull flow depth
p	protrusion
q_s	sediment flux
V_b	buried volume of grain of interest
C_V	volume correction ratio
V_o	sediment volume overlying grain of interest
z	distance from the bed
β	channel slope
ϕ_f	internal friction angle, effects of intergranular friction
ϕ_p	pivot angle
λ	bed porosity
ρ	water density
ρ_s	sediment density
τ_c^*	critical shear stress

Acknowledgments
Funding was provided by NSF awards CAREER-EAR0847799 and EAR1251785 to E. M. Yager and by EAR1734752 to M. W. Schmeeckle. Discussions with Todd Buxton and John Buffington helped to motivate this study. Laboratory/field assistance was provided by Andrew Tranmer, Claudia Bieler, and Christian Schär. Data are available through SEAD (https://sead2.ncsa.illinois.edu/datasets/5b4e3a7ce4b03951001f8fb0). We thank Rebecca Hodge, Allison Pfeiffer, Thomas Pähtz, and AE Christophe Ancey for their reviews of our paper.

References

Allan, A. F., & Frostick, L. (1999). Framework dilation, winnowing, and matrix particle size; the behavior of some sand-gravel mixtures in a laboratory flume. *Journal of Sedimentary Research*, *69*(1), 21–26. https://doi.org/10.2110/jsr.69.21

Ancey, C. (2010). Stochastic modeling in sediment dynamics: Exner equation for planar bed incipient bed load transport conditions. *Journal of Geophysical Research*, *115*, F00A11. https://doi.org/10.1029/2009JF001260

Bagherzadeh-Khalkhali, A., & Mirghasemi, A. A. (2009). Numerical and experimental direct shear tests for coarse-grained soils. *Particuology*, *7*(1), 83–91. https://doi.org/10.1016/j.partic.2008.11.006

Bandi, M. M., Rivera, M. K., Krzakala, F., & Ecke, R. E. (2013). Fragility and hysteretic creep in frictional granular jamming. *Physical Review E*, *87*(4), 042205. https://doi.org/10.1103/PhysRevE.87.042205

Bareither, C. A., Edil, T. B., Benson, C. H., & Mickelson, D. M. (2008). Geological and physical factors affecting the friction angle of compacted sands. *Journal of Geotechnical and Geoenvironmental Engineering*, *134*(10), 1476–1489. https://doi.org/10.1061/(ASCE)1090-0241(2008)134:10(1476)

Bertrand, T., Behringer, R. P., Chakraborty, B., O'Hern, C. S., & Shattuck, M. D. (2016). Protocol dependence of the jamming transition. *Physical Review E*, *93*(1), 012901. https://doi.org/10.1103/PhysRevE.93.012901

Bi, D., Zhang, J., Chakraborty, B., & Behringer, R. P. (2011). Jamming by shear. *Nature*, *480*(7377), 355–358. https://doi.org/10.1038/nature10667

Booth, A. M., Hurley, R., Lamb, M. P., & Andrade, J. E. (2014). Force chains as the link between particle and bulk friction angles in granular material. *Geophysical Research Letters*, *41*, 8862–8869. https://doi.org/10.1002/2014GL061981

Buffington, J. M., Dietrich, W. E., & Kirchner, J. W. (1992). Friction angle measurements on a naturally formed gravel streambed: Implications for critical boundary shear stress. *Water Resources Research*, *28*(2), 411–425. https://doi.org/10.1029/91WR02529

Buffington, J. M., & Montgomery, D. R. (1997). A systematic analysis of eight decades of incipient motion studies, with special reference to gravel-bedded rivers. *Water Resources Research*, *33*(8), 1993–2029. https://doi.org/10.1029/96WR03190

Buxton, T. H., Buffington, J. M., Yager, E. M., Hassan, M. A., & Fremier, A. K. (2015). The relative stability of salmon redds and unspawned streambeds. *Water Resources Research*, *51*, 6074–6092. https://doi.org/10.1002/2015WR016908

Celik, A. O., Diplas, P., & Dancey, C. L. (2013). Instantaneous turbulent forces and impulse on a rough bed: Implications for initiation of bed material movement. *Water Resources Research*, *49*, 2213–2227. https://doi.org/10.1002/wrcr.20210

Chang, K.-T., & Cheng, M.-C. (2014). Estimation of the shear strength of gravel deposits based on field investigated geological factors. *Engineering Geology*, *171*, 70–80. https://doi.org/10.1016/j.enggeo.2013.12.014

Chaudhuri, P., Berthier, L., & Sastry, S. (2010). Jamming transitions in amorphous packings of frictionless spheres occur over a continuous range of volume fractions. *Physical Review Letters*, *104*(16), 165701. https://doi.org/10.1103/PhysRevLett.104.165701

Ciamarra, M. P., Pastore, R., Nicodemi, M., & Coniglio, A. (2011). Jamming phase diagram for frictional particles. *Physical Review E*, *84*(4). https://doi.org/10.1103/PhysRevE.84.041308

Culshaw, M. G., Cripps, J. C., Bell, F. G., & Moon, C. F. (1991). Engineering geology of quaternary soils: I. Processes and properties. In *Quaternary engineering geology, Geological Society Engineering Geology Special Publication* (Vol. 7, pp. 3–28). https://doi.org/10.1144/GSL.ENG.1991.007.01.01

Dietrich, W. E. (1982). Settling velocity of natural particles. *Water Resources Research*, *18*(6), 1615–1626. https://doi.org/10.1029/WR018i006p01615

Dietrich, W. E., Kirchner, J. W., Ikeda, H., & Iseya, F. (1989). Sediment supply and the development of the coarse surface layer in gravel-bedded rivers. *Letters To Nature*, *340*(6230), 215–217. https://doi.org/10.1038/340215a0.

Diplas, P., Dancey, C. L., Celik, A. O., Valyrakis, M., Greer, K., & Akar, T. (2008). The role of impulse on the initiation of particle movement under turbulent flow conditions. *Science*, *322*(5902), 717–720. https://doi.org/10.1126/science.1158954

Espinosa, F. A., Rhodes, J. J., & McCullough, D. A. (1997). The failure of existing plans to protect Salmon habitat in the Clearwater National Forest in Idaho. *Journal of Environmental Management*, *49*, 205–230.

Estrada, N., Taboada, A., & Radjaï, F. (2008). Shear strength and force transmission in granular media with rolling resistance. *Physical Review E*, *78*(2), 021301. https://doi.org/10.1103/PhysRevE.78.021301

Farhadi, S., & Behringer, R. P. (2014). Dynamics of sheared ellipses and circular disks: Effects of particle shape. *Physical Review Letters*, *112*(14), 148301. https://doi.org/10.1103/PhysRevLett.112.148301

Fenton, J. D., & Abbott, J. E. (1977). Initial movement of grains on a stream bed: The effect of relative protrusion. *Proceedings of the Royal Society A: Mathematical, Physical and Engineering Sciences*, *352*(1671), 523–537. https://doi.org/10.1098/rspa.1977.0014

Hassan, M. A., & Reid, I. (1990). The influence of microform bed roughness elements on flow and sediment transport in gravel bed rivers. *Earth Surface Processes and Landforms*, *15*(8), 739–750. https://doi.org/10.1002/esp.3290150807

Haynes, H., & Pender, G. (2007). Stress history effects on graded bed stability. *Journal of Hydraulic Engineering*, *133*(4), 343–349. https://doi.org/10.1061/(ASCE)0733-9429(2007)133:4(343)

Hodge, R. A., Sear, D. A., & Leyland, J. (2013). Spatial variations in surface sediment structure in riffle-pool sequences: A preliminary test of the Differential Sediment Entrainment Hypothesis (DSEH). *Earth Surface Processes and Landforms*, *38*(5), 449–465. https://doi.org/10.1002/esp.3290

Isbash, S. V. (1936). Construction of dams by depositing rock in running water. In *Second congress on large dams* (pp. 123–136). Washington, DC.

Johnson, J. P. L. (2016). Gravel threshold of motion: A state function of sediment transport disequilibrium? *Earth Surface Dynamics*, *4*(3), 685–703. https://doi.org/10.5194/esurf-4-685-2016

Johnson, J. P. L., Aronovitz, A. C., & Kim, W. (2015). Coarser and rougher: Effects of fine gravel pulses on experimental step-pool channel morphodynamics. *Geophysical Research Letters*, *42*, 8432–8440. https://doi.org/10.1002/2015GL066097

Johnston, C. E., Andrews, E. D., & Pitlick, J. (1998). In situ determination of particle friction angles of fluvial gravels. *Water Resources Research*, *34*(8), 2017–2030. https://doi.org/10.1029/98WR00312

Kirchner, J. W., Dietrich, W. E., Iseya, F., & Ikeda, H. (1990). The variability of critical shear stress, friction angle, and grain protrusion in water-worked sediments. *Sedimentology*, *37*(4), 647–672. https://doi.org/10.1111/j.1365-3091.1990.tb00627.x

Kloss, C., Goniva, C., Hager, A., Amberger, S., & Pirker, S. (2012). Models, algorithms and validation for opensource DEM and CFD-DEM. *Progress in Computational Fluid Dynamics, An International Journal*, *12*(2/3), 140–152. https://doi.org/10.1504/PCFD.2012.047457

Kothyari, U. C., & Jain, R. K. (2008). Influence of cohesion on the incipient motion condition of sediment mixtures. *Water Resources Research*, *44*, W04410. https://doi.org/10.1029/2007WR006326

Kumar, N., & Luding, S. (2016). Memory of jamming? Multiscale models for soft and granular matter. *Granular Matter*, *18*(3), 1–21. https://doi.org/10.1007/s10035-016-0624-2

Lamb, M. P., Dietrich, W. E., & Venditti, J. G. (2008). Is the critical Shields stress for incipient sediment motion dependent on channel-bed slope? *Journal of Geophysical Research*, *113*, F02008. https://doi.org/10.1029/2007JF000831

Lambe, T. W., & Whitman, R. V. (1969). *Soil mechanics*. New York: John Wiley & Sons.

Leary, K. C. P., & Schmeeckle, M. W. (2017). The importance of splat events to the spatiotemporal structure of near-bed fluid velocity and bedload motion over bedforms: Laboratory experiments downstream of a backward-facing step. *Journal of Geophysical Research: Earth Surface*, *122*, 2411–2430. https://doi.org/10.1002/2016JF004072

Lee, D. B., & Jerolmack, D. (2018). Scales of collective entrainment and intermittent transport in collision-driven bed load. *Earth Surface Dynamics Discussions*, *6*, 1–21. https://doi.org/10.5194/esurf-2018-8

Li, Z., & Komar, P. D. (1986). Laboratory measurements of pivoting angles for applications to selective entrainment of gravel in a current. *Sedimentology*, *33*(3), 413–423. https://doi.org/10.1111/j.1365-3091.1986.tb00545.x

Lin, P. S., Yang, L. W., & Juang, C. (1998). Subgrade reaction and load-settlement characteristics of gravelly cobble deposits by plate-load tests. *Canadian Geotechnical Journal*, *35*(5), 801–810. https://doi.org/10.1139/t98-044

Madej, M., Sutherland, D., Lisle, T., & Pryor, B. (2009). Channel responses to varying sediment input: A flume experiment modeled after Redwood Creek, California. *Geomorphology*, *103*(4), 507–519. https://doi.org/10.1016/j.geomorph.2008.07.017

Masteller, C. C., & Finnegan, N. J. (2017). Interplay between grain protrusion and sediment entrainment in an experimental flume. *Journal of Geophysical Research: Earth Surface*, *122*, 274–289. https://doi.org/10.1002/2016JF003943

Meyer-Peter, E., & Müller, R. (1948). Formulas for bed-load transport. In *Proc., 2nd Meeting, IAHR* (pp. 39–64). Stockholm, Sweden.

Mollanouri Shamsi, M. M., & Mirghasemi, A. A. (2012). Numerical simulation of 3D semi-real-shaped granular particle assembly. *Powder Technology*, *221*, 431–446. https://doi.org/10.1016/j.powtec.2012.01.042

Mueller, E. R., Pitlick, J., & Nelson, J. M. (2005). Variation in the reference Shields stress for bed load transport in gravel-bed streams and rivers. *Water Resources Research*, *41*, W04006. https://doi.org/10.1029/2004WR003692

Ockelford, A.-M., & Haynes, H. (2013). The impact of stress history on bed structure. *Earth Surface Processes and Landforms*, *38*(7), 717–727. https://doi.org/10.1002/esp.3348

Pähtz, T., & Durán, O. (2017). Fluid forces or impacts: What governs the entrainment of soil particles in sediment transport mediated by a Newtonian fluid? *Physical Review Fluids*, *2*(7), 074303. https://doi.org/10.1103/PhysRevFluids.2.074303

Pähtz, T., & Durán, O. (2018). The cessation threshold of nonsuspended sediment transport across aeolian and fluvial environments. *Journal of Geophysical Research: Earth Surface*, *123*, 1638–1666. https://doi.org/10.1029/2017JF004580

Paphitis, D., & Collins, M. B. (2005). Sand grain threshold, in relation to bed "stress history": An experimental study. *Sedimentology*, *52*(4), 827–838. https://doi.org/10.1111/j.1365-3091.2005.00710.x

Perret, E., Berni, C., Camenen, B., Herrero, A., & El Kadi Abderrezzak, K. (2018). Transport of moderately sorted gravel at low bed shear stresses: The role of fine sediment infiltration. *Earth Surface Processes and Landforms*, *43*(7), 1416–1430. https://doi.org/10.1002/esp.4322

Petrosky, C. E., Holubetz, T. B., & Everson, L. B. (1988). Idaho habitat evaluation for off-site mitigation Record Annual Report 1987 (No. Contract No. DE-A179-84BP13381, Project 83–7). Idaho Department of Fish and Game.

Prancevic, J. P., & Lamb, M. P. (2015). Particle friction angles in steep mountain channels: Friction angles in mountain channels. *Journal of Geophysical Research: Earth Surface*, *120*, 242–259. https://doi.org/10.1002/2014JF003286

Recking, A. (2009). Theoretical development on the effects of changing flow hydraulics on incipient bed load motion. *Water Resources Research*, *45*, W04401. https://doi.org/10.1029/2008WR006826

Reid, I., Frostick, L. E., & Layman, J. T. (1985). The incidence and nature of bedload transport during flood flows in coarse-grained alluvial channels. *Earth Surface Processes and Landforms*, *10*(1), 33–44. https://doi.org/10.1002/esp.3290100107

Reneau, S. L., Katzman, D., Kuyumjian, G. A., Lavine, A., & Malmon, D. V. (2007). Sediment delivery after a wildfire. *Geology*, *35*(2), 151. https://doi.org/10.1130/G23288A.1

Richards, C., & Cernera, P. J. (1987). Salmon river habitat enhancement, Annual report FY 1986. US Department of Energy, BPA, Division of Fish and Wildlife.

Sanguinito, S., & Johnson, J. (2012). Quantifying gravel overlap and dislodgement forces on natural river bars: Implications for particle entrainment. *Earth Surface Processes and Landforms*, *37*(1), 134–141. https://doi.org/10.1002/esp.2237

Schmeeckle, M. W. (2014). Numerical simulation of turbulence and sediment transport of medium sand. *Journal of Geophysical Research: Earth Surface*, *119*, 1240–1262. https://doi.org/10.1002/2013JF002911

Schmeeckle, M. W. (2015). The role of velocity, pressure, and bed stress fluctuations in bed load transport over bed forms: Numerical simulation downstream of a backward-facing step. *Earth Surface Dynamics*, *3*(1), 105–112. https://doi.org/10.5194/esurf-3-105-2015

Schmeeckle, M. W., Nelson, J. M., & Shreve, R. L. (2007). Forces on stationary particles in near-bed turbulent flows. *Journal of Geophysical Research*, *112*, F02003. https://doi.org/10.1029/2006JF000536

Sennatt, K. M., Salant, N. L., Renshaw, C. E., & Magilligan, F. J. (2006). Assessment of methods for measuring embeddedness: Application to sedimentation in flow regulated streams. *Journal of the American Water Resources Association*, *42*(6), 1671–1682. https://doi.org/10.1111/j.1752-1688.2006.tb06028.x

Shvidchenko, A. B., Pender, G., & Hoey, T. B. (2001). Critical shear stress for incipient motion of sand/gravel streambeds. *Water Resources Research*, *37*(8), 2273–2283. https://doi.org/10.1029/2000WR000036

Silbert, L. E. (2010). Jamming of frictional spheres and random loose packing. *Soft Matter*, *6*(13), 2918. https://doi.org/10.1039/c001973a

Simoni, A., & Houlsby, G. T. (2006). The direct shear strength and dilatancy of sand–gravel mixtures. *Geotechnical and Geological Engineering*, *24*(3), 523–549. https://doi.org/10.1007/s10706-004-5832-6

Song, C., Wang, P., & Makse, H. A. (2008). A phase diagram for jammed matter. *Nature*, *453*(7195), 629–632. https://doi.org/10.1038/nature06981

Strom, K., Papanicolaou, A. N., Evangelopoulos, N., & Odeh, M. (2004). Microforms in gravel bed rivers: Formation, disintegration, and effects on bedload transport. *Journal of Hydraulic Engineering*, *130*(6), 554. https://doi.org/10.1061/(ASCE)0733-9429(2004)130:6(554)–567.

Torquato, S., & Stillinger, F. H. (2010). Jammed hard-particle packings: From Kepler to Bernal and beyond. *Reviews of Modern Physics*, *82*(3), 2633–2672. https://doi.org/10.1103/RevModPhys.82.2633

Trulsson, M. (2018). Rheology and shear jamming of frictional ellipses. *Journal of Fluid Mechanics*, *849*, 718–740. https://doi.org/10.1017/jfm.2018.420

Turowski, J. M., Badoux, A., & Rickenmann, D. (2011). Start and end of bedload transport in gravel-bed streams. *Geophysical Research Letters*, *38*, L04401. https://doi.org/10.1029/2010GL046558

US Bureau of Land Management (1996). *Challis Resource Area, Draft Resource Management Plan and Environmental Impact Statement* (Vol. 3, p. 606). Salmon, ID: US BLM, Challis Resource Area, Upper Columbia Salmon Clearwater Districts.

USDA Forest Service (2002). *Middle-black analysis, final environmental impact statement*. Clearwater Country, ID: Clearwater National Forest, North Fork Ranger District.

USDA Forest Service (2005). *Red Pines final environmental impact statement*. Idaho County, ID: Nez Perce National Forest, Red River Ranger District.

USDA Forest Service (2014). *Nez Perce–Clearwater National Forests forest plan assessment (No. 1.0 Terrestrial and Aquatic Ecosystems and Watersheds)* (p. 162). Nez Perce-Clearwater National Forest.

Valyrakis, M., Diplas, P., & Dancey, C. L. (2013). Entrainment of coarse particles in turbulent flows: An energy approach. *Journal of Geophysical Research: Earth Surface*, *118*, 42–53. https://doi.org/10.1029/2012JF002354

Valyrakis, M., Diplas, P., Dancey, C. L., Greer, K., & Celik, A. O. (2010). Role of instantaneous force magnitude and duration on particle entrainment. *Journal of Geophysical Research*, *115*, F02006. https://doi.org/10.1029/2008JF001247

Vollmer, S., & Kleinhans, M. G. (2007). Predicting incipient motion, including the effect of turbulent pressure fluctuations in the bed. *Water Resources Research*, *43*, W05410. https://doi.org/10.1029/2006WR004919

Vowinckel, B., Jain, R., Kempe, T., & Fröhlich, J. (2016). Entrainment of single particles in a turbulent open-channel flow: A numerical study. *Journal of Hydraulic Research*, *54*(2), 158–171. https://doi.org/10.1080/00221686.2016.1140683

Wiberg, P. L., & Smith, J. D. (1987). Calculations of the critical shear stress for motion of uniform and heterogeneous sediments. *Water Resources Research*, *23*(8), 1471–1480. https://doi.org/10.1029/WR023i008p01471

Yager, E. M., Kirchner, J. W., & Dietrich, W. E. (2007). Calculating bed load transport in steep boulder bed channels. *Water Resources Research*, *43*, W07418. https://doi.org/10.1029/2006WR005432

Yager, E. M., Turowski, J. M., Rickenmann, D., & McArdell, B. W. (2012). Sediment supply, grain protrusion, and bedload transport in mountain streams. *Geophysical Research Letters*, *39*, L10402. https://doi.org/10.1029/2012GL051654

Zhang, J., Majmudar, T. S., Sperl, M., & Behringer, R. P. (2010). Jamming for a 2D granular material. *Soft Matter*, *6*(13), 2982. https://doi.org/10.1039/c000147c

Zhuang, L., Nakata, Y., Kim, U.-G., & Kim, D. (2014). Influence of relative density, particle shape, and stress path on the plane strain compression behavior of granular materials. *Acta Geotechnica*, *9*(2), 241–255. https://doi.org/10.1007/s11440-013-0253-4